

Efficient Building Detection for Large-scale Urban Remote Sensing

Feiyu Qin, Tongcun Zuo, Xuejin Chen

Abstract—Extracting buildings from remote sensing images plays an important role in urban applications (e.g., urban planning and digital city). However, this task is quite difficult due to the great diversity of buildings and similarities between buildings and other categories. Recent approaches have attempted to harness the capabilities of deep learning techniques for building extraction. In this paper, we propose a robust method which extracts buildings from large-scale remote sensing images efficiently via deep learning. And further we extend our method to the 3D building reconstruction to accelerate the overall process. Our study demonstrates that learning low-level appearance information and high-level semantic information are equally important in building extraction task since buildings possess various scales and aspect ratios in the scene. Hence, to make full use of the information extracted from each layer, we propose a simple but effective hierarchical fusion operation which fuses the feature maps between channels stage by stage. In this paper, a novel network named hierarchical fused fully convolution network(HF-FCN) is also described which fuses the information through combining the fusion operations to the general networks. The experiments on several available remote sensing image datasets show that our method achieves state-of-the-art performance. (xuejin:Problem: Over-emphasized the building detection part, without clearly describe the scope of this paper and the relationship between detection and reconstruction.)

Index Terms—building extraction, hierarchical fusion operation, Hierarchically Fused Fully Convolutional Network (HF-FCN), 3D city modelling

I. INTRODUCTION

(xuejin: Is your goal reconstruction or building extraction? The introduction should explain the overall goal. What are the challenges for building modeling from remote sensing images? What kind of work has been done in the literature? Why do we focus on building detection? What are our contributions?)

BUILDING extraction, which aims to extract rooftop¹ in a large-scale remote sensing image, remains one of the fundamental challenges have been studied for decades in the field of remote sensing. Moreover, auto extraction of building rooftops from aerial and satellite imagery is an important step in many applications, such as: urban planing, automated map making, 3D city modeling, updating geographical dataset and military reconnaissance. But, it is particularly difficult to extract rooftop at the pixel level for the following reasons:

- Different density of buildings in the scene. A rural scene has low density but an urban scene has high density, with a suburban scene in between (medium density).

¹Because the data sets used in our article are high altitude remote sensing images which could be considered as the top views of the ground. Therefore, we do not distinguish the concepts of buildings and rooftops in the subsequent description.



Fig. 1. Examples of remote sensing patches with different kinds of challenges. (a) Shadow occlusion in green frame. (b) Low inter-class differences. (c) High intra class variance. (d) A lot of tiny buildings close to each other.

- Diverse shapes of the buildings. Buildings come in many shapes from simple rectangular blocks with flat roof to complex shapes with intricate roof shape.
- The quality of remote sensing images. Images vary in terms of contrast, resolution, and image principle [1].

Several patches are shown in Fig. 1 (xuejin:do not use the figure no directly, using ref.), which illustrate the different challenges of building extraction task.

In the past decades, many researchers have made effort to extract buildings automatically. At first, many simple knowledge-based methods were put forward by [1], [2], [3], [4], [5]. Their basic ideas are derived from prior knowledge that buildings are closed polygons made up of some straight lines. Some others are energy-based methods including the variational level set evolution, improved snake model and graph cut [6], [7], [8]. Due to early methods depend too much on prior and initialization. It does not apply to building extraction of complex scene.

In recent years, with the development of machine learning, many techniques via machine learning are gradually introduced into the remote sensing domain. At first, some shallow networks were proposed for multiple geographic object extraction [9], [10], [11], [12]. Since methods use patches for segmentation, they are inefficient and inaccurate for the pixel-wise segmentation task. Further, with the growth of computer power, deep learning developed rapidly and brought into the field of remote sensing. Some researchers tried deep learning for aerial images classification and semantic pixel labelling [13], [14], [15], [16], [17]. Unfortunately, owing to ignoring the hierarchical information extracted by the network, they could not deal with the case that scenes of close-packed buildings well.

To fix the above problems, a relatively simple, but very effective fusion operation is proposed in this work. And it could be combined into a general CNN architecture easily for building extraction. Differ from above mentioned methods, we take full advantages of the low-level appearance information

as well as high-level semantic information by the novel fusion operation in a way of stage by stage. Inspired by FCN [18] whose output is in the same resolution of input, we propose a novel hierarchically fused FCN, named HF-FCN for buildings pixel-wise classification. Differ from the traditional FCN, a set of hierarchical fusion operations are used to fuse the intra layer information and inter layer information respectively which improve the performance of FCN greatly. And numerous experiments conducted on three remote sensing image datasets all obtain fairly good results. Further, we extend our work to the field of 3D modeling as the part of building detection. It is easily integrated into the pipeline of building reconstruction and achieve good performance. Our technical contributions are:

- 1) A effective hierarchical fusion operation which is specially designed for multi-scale building extraction is proposed. Combining with a general FCN, a novel network is presented, named HF-FCN that can deal with the problems of different sizes, diverse appearance and mutual occlusion of buildings and etc.
- 2) HF-FCN is an end-to-end network that does not need any post processing. And the approach is significantly computationally efficient than existing techniques. Besides, the overall accuracy based on HF-FCN exceeds the state-of-art algorithms.

The remainder of this paper is organized as follows. Sec. II sums up the related works in the past. In Sec. III, we introduce the fusion operation and architecture of HF-FCN. The training loss are also presented. And in Sec. IV, a brief description of the dataset used for our task is provided. HF-FCN training strategies, details and its evaluation metrics are also described. In Sec. V, we display and analysis the experimental results. Extension in 3D building modeling are presented in Sec. VI. Finally, the conclusion is discussed in Sec. VII.

II. RELATED WORK

Building extraction is one of the most fundamental problems in remote sensing domain, which has been studied for nearly 30 years. As time goes by, many research achievements have sprung up. We roughly divide these methods into three groups: one is based on the shape prior, another is based on the energy function and machine learning third. Meanwhile, the methods of machine learning could be divided into two parts: one is shallow networks and the other is deep learning methods. Here we briefly review some representative methods that have evolved in the past decades in the different groups respectively. Moreover, several related work which are popular in computer vision domain similar to our task are also introduced. (xuejin:More related work on city modeling/urban modeling. Maybe facade modeling.)

Shape Prior based Methods During early days, methods are mainly based on the hypothesis of prior knowledge. Huertas and Nevatia [1] assumed that buildings are rectangular or composed of rectangular components. Based on it, the approach detected lines and corners, traced object boundaries and used shadows to verify. Later, a system [2] for building detection and modelling was proposed with the assumption

that the roofs were flat or symmetrical and walls were vertical. With known ground height and detected rooftop, the reconstructed models could be soon obtained. Further, Noronha and Nosrati [3] transformed the line and intersection points in remote sensing images into a graph presentation, and turned the problem of polygon finding into the one that finding loops in the graph. It was still estimated on assumption that the buildings are polygonal. Later, Izadi and Saeedi [4] presented a complete system for building detection and modelling. In the stage of extracting buildings, a tree consisting of intersection points of lines was created and refined according to the found hypotheses. The sun azimuth and elevation angles were used to estimate the height with existing shadows afterwards. In recent years, very high resolution (VHR) optical satellite imagery could be obtained easily. Based on it, Wang et al [5] proposed an efficient method for automatic rectangular building extraction by detecting line segments and grouping them based on path integrity and closed contour. Nevertheless, the method depends on the clear remote sensing images and accurate line segmentation heavily. (xuejin:If there are two authors, say A and B proposed.... if more than two authors, say A et al ..)

The aforementioned shape-based methods have a good performance in rural scenes with low density of buildings. Nevertheless, there are several limitations of these methods. First, the shape-based methods inherently limited to handle buildings of arbitrary shapes. Second, they may fail to deal with complicated cases, for instance, buildings are close to each other, which thereby is hard to adapt to today's applications. Third, the algorithms using shadows to verify corners and estimate height are greatly limited by obvious shadows and sparse building environment.

Energy Function based Methods Later, several energy-based methods in image segmentation domain have been applied to automatic rooftop extraction. Cote and Saeedi [6] proposed a level set evolution method that employed detected corners as endpoints of the initial curves. Peng et al [7] used an improved snake model to refine the coarse segmentation results. Later, the urban-region-detection problems were casted as one of multiple subgraph matching by Sirmacek and Unsalan [8]. They considered each SIFT keypoint as a vertex, neighborhood between vertexes as edges of the graph and converted the original image segmentation problem into a graph-cut optimization process.

Experiment results displayed in the above works reveal that energy-based methods limit by a good initialization. And it is generally known that energy-based methods are greatly influenced by the nature of the images. That is to say, the above mentioned methods are not applicable to the situation where high altitude remote sensing images of intensive buildings with severe shadow occlusion.

Shallow Networks Over the past decade, machine learning have achieved great success in the field of computer vision. And there are significant amount of efforts on building extraction task via machine learning. At first, Mnih [9] proposed a shallow patch-based network which has five layers with a 64 by 64 aerial patch as input. The output of the network was processed by conditional random fields (CRFs) to constrain the

segmentation continuity. Afterwards, Satio et al. [10] put forward two major strategies to improve the performance of [9]. The one was a channel-wise inhibited softmax (CIS) for getting a multi-label prediction result, the other was model averaging (MA) with spatial displacement for enhancing the prediction result. Later, Alshehhi et al. [11] adjusted the architecture of [9] through changing the kernel size of convolutional layers and replacing the last fully connection layer with the average pooling layer. Alternative post-processing strategies such as CRFs and multi-scales were also used to improve the final prediction results. At the same time, some other methods took advantage of the feature extraction capability of CNNs to generate feature descriptions of patches for further segmentation; for instance, Paisitkriangkrai et al. [13] made use of both the CNN and hand-craft extracted features and combined them together to generate predicted labels of each patch. The CRFs was also used as post-processing to get a sound result. Unlike [13], [17] put forward a multi-label pixelwise classification method using the feature vector extracted by a CNN to train a Support Vector Machine (SVM) for classification. Other appearance information, such as edges [12] are also harnessed to guide the shallow network to extract buildings.

Although the above mentioned methods have exceeded the traditional methods, there are still several disadvantages. (a) The methods using shallow networks always cast the problem of building segmentation as a patch classification problem. It has a great impact on the segmentation accuracy. (b) Most of them are processed by at least one kind of post-processing, which is time-consuming.

Deep Learning More recently, Long et al. [18] illustrated that Fully Convolutional Networks (FCN) handle the problem of multi-label pixel-wise classification better. Hence, Liu et al. [14] did a further research on the formulation proposed by Paisitkriangkrai [13] but with FCN instead of shallow network and applied a higher-order CRFs as post-processing. Unlike traditional CRFs, the label consistency for the pixels within the same segment were enforced by higher-order CRFs. In order to reduce the information loss during pooling stage and accelerate the decoding of FCN, SegNet [19] delivered pooling indices computed in the max-pooling to the decoder. It eliminated the need of learning during the up-sample stage and retained partial information during pooling stage while preserving segmentation performance well. Accordingly, Audebert et al. [15] used SegNet architecture for semantic labeling of remote sensing images and got better prediction results compared to the traditional methods. Later, Kampffmeyer et al. [16] proposed a novel idea that using CNN with missing data for urban land cover classification. The idea is came from a modality hallucination architecture proposed by Hoffman et al. [20] which solved the problem that missing some kinds of data during test process.

Above-mentioned deep learning models have exceeded the traditional methods significantly, but most of them completely ignored important hierarchical features encoded in the CNNs. But for building extraction task, the lost low-level and middle-level information are critical to the final segmentation result.

Computer Vision In the filed of computer vision, the

FCNs [18] were introduced as a powerful method for semantic segmentation and already achieved great success. But, along with the deepening of network, the feature maps with lower resolution which causes the segmentation accuracy decline. In order to weaken the influence caused by deepen of network, Chen et al. [21] proposed a atrous convolution which enlarged the receptive field and reduced the number of pooling layers at the same time. Vemulapalli et al. [22] further extended the Deeplab [21] with a pairwise network and proposed a Gaussian Conditional Random Field Network for more continuous segmentation results. Afterwards, with the advent of the powerful networks such as ResNet [23], GoogLeNet [24] and their variants [25] [26] [27], a large amount of literature made use of these networks as their main structure for semantic segmentation. Zhao et al. [12] recently developed a pyramid pooling module following the ResNet [23] to get multi-scale feature maps and connected them with the feature maps which before pyramid pooling to create the final prediction. Zuo et al. [28] described a hierarchically fused fully convolutional network, which combined the feature maps from each group of VGG16 Net to generate the final prediction. In this paper, we extend the work of [28] and proposed a simple but effective fusion operation that could be easily combined to the general network. We also explore the effect of different layers of features on the final result. The details of our idea will be described in the next section.

The most related work are U-Net [29] and FPN [30]. They both exploited the information from different layers. Differ from the U-Net which simple concatenated the feature maps from encoder to decoder, we apply a fusion operation firstly to fuse the feature maps created in the same convolution layers in the path of encoder to get more richer features. The main idea of FPN was leveraging the encoder part as a feature pyramid, with predictions made independently at all levels. During the top-down path of FPN, it only exploited the feature maps which were came from last residual block of each stage, but we take advantage of the all feature maps from the each stage. Moreover, we upsample the feature maps from each stage to the same resolution of the input and apply a hierarchical fusion operation to fuse the upsampled feature maps to a final prediction instead of directly predicting from each stage. That is to say, we only make a prediction rather than multiple predictions.

(xuejin:Need a paragraph to discuss recent semantic segmentation networks.)

(xuejin:Also cite our accv paper and describe the relationship/difference of this journal paper with it.)

III. HIERARCHICALLY FUSED FULLY CONVOLUTIONAL NETWORK

In this section, we introduce a novel operation for feature fusion, named hierarchical fusion operation and apply it to the common networks, VGG16 Net and ResNet. The overview diagram in Fig. 2 shows where the fusion operations take effect and how they work. Different from other networks for semantic segmentation, we apply the fusion operation twice to integrate information gradually. Our network consists of

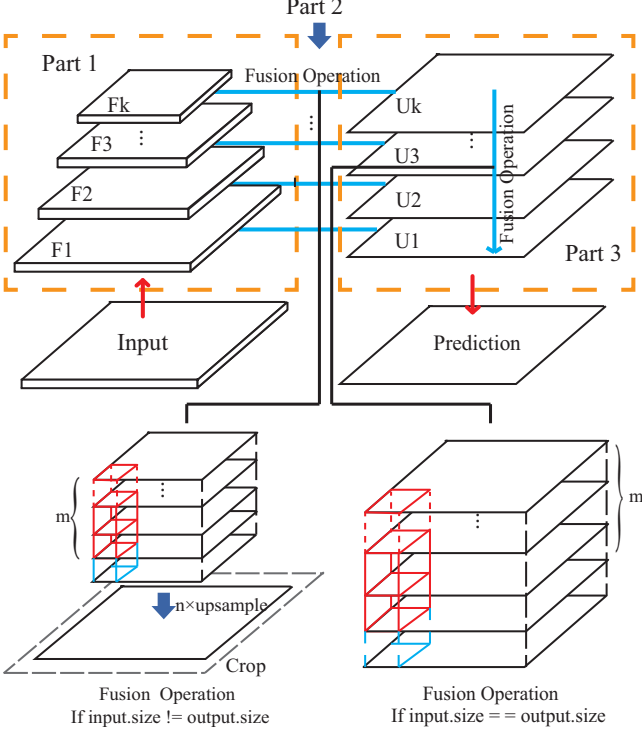


Fig. 2. The first line shows the overview of our network. The second row shows the details of two kinds of fusion operation. One is a case where the input is not equal to the output and the other is the input equal to the output. \$F_k\$ means the feature maps come from the \$k\$th layer. \$m\$ for number of feature maps. \$n\$ said the \$n\$ times of up sampling.

three parts. Part 1 is a bottom-up pathway which plays a role of features extractors at different levels. In theory, arbitrary feature extraction network is applicable to the Part 1. The second part is a process of feature fusion in the first stage, which fuses the feature maps generated from Part 1. Besides, Part 3 is a second stage of feature fusion. In Part 3, we take full advantage of the information extracted from the Part 2 by learning the connection weights between upsampled feature maps.

(xuejin:Put overview here. Explain the main components of our methods.)

A. Network Architecture

Part 1 The Part 1 is a bottom-up pathway, which generates the hierarchical feature maps from the network. With the increase of the field of perception, the extracted semantic information is gradually from the lower level to the high level. At the same time, the extracted information of image is from local to global. Each group of feature maps come from the same feature extractor contribute to the \$\{F_k\}\$ in Fig. 2, where \$k : \Omega \rightarrow \{1, \dots, K\}\$. And \$K\$ is group number of feature maps; for instance, \$K\$ is 13 for VGG16 Net that we consider each convolution(conv) layer as a feature extractor. Specifically, for ResNets, we consider a ResBlock as a feature extractor that \$K\$ is 15.

Part 2 The Part 2 which fuses the feature maps of each group extracted from Part 1 via a set of hierarchical fusion operations. Due to the feature maps learned from same group including similar types of information, we fuse them into

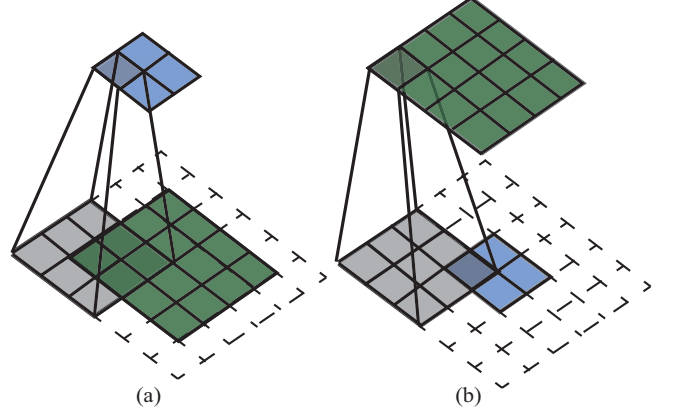


Fig. 3. A diagram of convolution and transposed convolution. The traditional convolution and transposed convolution are shown in the left and right column, respectively. The input of convolution is \$4 \times 4\$, the output is \$2 \times 2\$ and the kernel is \$3 \times 3\$. And the transposed convolution is the opposite.

one feature map, which contains richer information. The hierarchical fusion operation consists of three steps: A \$1 \times 1\$ conv layer first, a deconvolutional (transposed convolution) layer second and crop operation third. The Part 2 in Fig. 2 can be written as:

$$U_k = Crop(UpSample_n(Conv(\{F_k\}))) \quad (1)$$

where \$\{F_k\}\$ is a set of extracted feature maps from Part 1, \$k : \Omega \rightarrow \{1, \dots, K\}\$.

The first step is a \$1 \times 1\$ conv operation among the channels of feature maps in the same group. \$Y = Conv(\{X\})\$ is defined as:

$$Y(i, j) = \sum_{m=1}^M w_m X_m(i, j) \quad (2)$$

where \$M\$ is the number of the feature maps in \$\{X\}\$. The \$w_m\$ is the weight of conv kernels, \$m : \Omega \rightarrow \{1, \dots, M\}\$.

If the input and output were to be unrolled into vectors form left to right, top to bottom, the convolution operation can be expressed as:

$$y = Wx \quad (3)$$

where \$x, y\$ are flattened vector of input and output. The \$W\$ is a sparse matrix whose non-zero elements are weights of kernels. A diagram of conv operation is shown in Fig. 3(a). For Fig. 3(a), \$x\$ is a 16-dimensional vector (the input \$X\$ is a \$4 \times 4\$ patch), \$y\$ is a 4-dimensional vector and \$W\$ is a matrix of \$4 \times 16\$.

The output of \$Conv\{\{F_k\}\}\$ are upsampled by a transposed convolution which is written as \$Y = UpSample_n(X)\$, where \$n\$ means \$n\$ times up sampling. The \$n\$ in our network is determined by the size of input \$X\$ and output \$Y\$ that is equal to \$\max\{[Y.weight/X.weight], [Y.height/X.height]\}\$. Contrary to conv operation, the transposed conv is a process of transforming the features of low dimension to high dimension. It can be written in a inverse form of conv operation:

$$y = W_1^T x \quad (4)$$

where \$x, y\$ are flattened vector of input and output. The \$W_1^T\$ is a sparse matrix whose non-zeros elements are weights of deconvolutional kernels. Fig. 3(b) shows a diagram of

transposed conv. For Fig. 3(b), x is 4-dimensional vector (the input X of transpose conv is a 2×2 patch), y is a 16-dimensional vector and W_1^T is a matrix of 4×16 .

The W_1^T of transposed conv layers of different groups are learned separately. It means that the transposed conv layers recovery semantic information from hierarchical feature maps. The $Crop(\{X\})$ operation in Part 2 is just a center alignment crop which cuts the superfluous boundary of upsampled feature maps. The output $\{U_k\}$, $k : \Omega \rightarrow \{1, \dots, K\}$ of Part 2 are in the same resolution of the network input.

Part 3 Part 3 is the second fusion stage which aims to fuse the cropped feature maps from Part 2. In this part, the fusion operation plays a role of feature weighting. Using a 1×1 conv layer, a set of parameters w_k , $k : \Omega \rightarrow \{1, \dots, K\}$ are learned to combine the hierarchical feature maps. The expression of the Part 3 is as follows:

$$Y = Conv(\{U_k\}) \quad (5)$$

where Y is output feature map. $\{U_k\}$ is input of Part 3 and output of Part 2.

In order to get a probability map of input, the output Y of Part 3 is normalized by a sigmoid function:

$$S(x) = \frac{1}{1 + e^{-x}} \quad (6)$$

After normalization, A probability map P of rooftop is generated, each point in P means the probability that pixel belongs to a rooftop. If the pixel $x(i, j)$ belongs to a rooftop, the output $P(i, j) \approx 1$.

B. Network Training

The ground truth G in our dataset is labeled by 0 or 1 to indicate whether a pixel belongs to a roof or not. (**xuejin:only roof? or part of the building including facades?**) When a remote sensing image X is inputted into the network, the output is a prediction probability map $P(X; W)$ of roof, where W denotes all the parameters that learned by HF-FCN including first part, Part 2 and 3. We use the sigmoid cross-entropy loss function to penalize each position on the prediction map formulated as:

$$L(W) = -\frac{1}{|I|} \sum_{i=1}^{|I|} [\tilde{g}_i \log P(X_i; W) + (1 - \tilde{g}_i) \log(1 - P(X_i; W))] \quad (7)$$

where \tilde{g}_i is label of X_i , $i : \Omega \rightarrow \{1, \dots, |I|\}$, $|I|$ is the number of pixels in the input image X .

IV. EXPERIMENTS

To verify the effectiveness of the proposed network, extensive experiments have been conducted on three remote sensing datasets. In this section, the experimental setups are described including details of datasets, training settings of HF-FCN and different criterions for evaluation.

A. Dataset Description

a) *Massachusetts dataset*: Massachusetts dataset consists of 151 aerial images of the Boston area which covers roughly 340 square kilometers. The resolution of each image is 1500×1500 with the spacial resolution of 1 meter per pixel. And the

images are composed of red, green and blue channels. This dataset is built by Mnih while ground-truth is produced by Saito et al. The dataset is split into three parts, a training set of 137 images, a test set of 10 images and validation set of 4 images. To train the network, we create a set of image tiles for training and validation by sliding a 256×256 window with 64 stride from right to left, top to bottom. The detailed description is shown in Table I.

b) *Vaihingen dataset*: Vaihingen dataset is captured over Vaihingen which is a relatively small village with many detached buildings and small multi story buildings in Germany. This dataset contains 16 labeled images whose spacial resolution is 9cm per pixel. It consists of near infra-red, red, green, blue imagery with corresponding normalized digital surface models (nDSMs) and raw DSMs. The dataset is divided into training set, validation set, and test set which have 11 images, 2 images, and 3 images respectively. The same crop operations are done as the Massachusetts dataset.

c) *Potsdam dataset*: In the Potsdam dataset, there are 24 labeled images whose ground sampling distance is 5cm. This dataset shows a typical historic city with large building blocks. In order to grasp the global information of the building, the spacial resolution of the original image is reduced from 6000×6000 to 1500×1500 . Each image in this dataset contains 5-channel information: red, green, yellow, DSM and nDSM. We split the dataset into training, validation and test sets in a proportion of 7 : 2 : 1.

Some measures of data augmentation including data rotation and mirror flipping are made on the three datasets. Due to the other methods using dataset a) do not extend the dataset, so the predict results on the original and extensible dataset a) are both presented to make a fair comparison. Besides, the data quantity of dataset b) and c) is not enough to make a adequate training, so we used the extensible dataset as our training set directly. The components of the datasets are listed in Table I. And some sampled patches of dataset a), b), c) are shown in Fig. 4. The characteristics and challenges of the three datasets are:

- The dataset a) has a lot of intensive buildings, which causes great difficulties for the separation of buildings.
- There is an obvious shadow occlusion in dataset b) which may lead to a wrong segmentation in the part of the shadowed rooftop.
- Large intra class differences and small inter class differences are presented in dataset c). One building consists of several materials while the roads and buildings are the similar colour.

B. Training Settings

HF-FCN is trained on dataset a) firstly owing to large amounts of training data. The pre-trained model of VGG16 Net and ResNet are used to finetune our HF-FCN. We use the stochastic gradient descent algorithm with the learning rate divided by 10 for each 8000 iterations to train our network. The drop-out ratio is set to 0.5 which avoids overfitting. When the HF-FCN converges on the dataset a), we transfer it to the

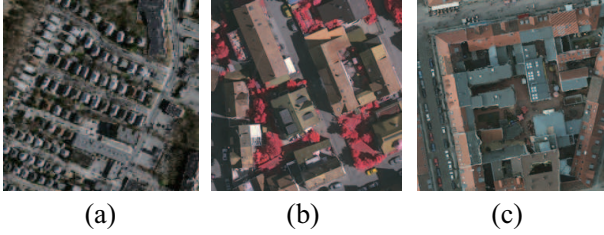


Fig. 4. Sample patches on the three datasets (a) Massachusetts dataset (b) Vaihingen dataset (c) Potsdam dataset

TABLE I
COMPOSITIONS OF DATASETS

	Massachusetts	Vaihingen	Potsdam
Labeled images	151	16	24
GSD	1m	9cm	5cm
Bands	R,G,B	IR,R,G,DSM	IR,R,G,B,DSM
Training images	137	11	17
Training patches	75938	115088	85000
Training patch size	256×256	256×256	256×256
Validation images	4	3	4
validation patches	2500	28376	25000
Validation patch size	256×256	256×256	256×256
Test images	10	2	3

other datasets. All experiments in this paper are performed using the deep learning framework Caffe and trained on a single NVIDIA Titan 12GB GPU. Besides, the hyper-parameters are listed in Table II (xuejin:III).

C. Evaluation Metrics

Several evaluation metrics are adopted in our work. For dataset *a*), the most common metrics are correctness (precision) and completeness (recall). The standard ($\rho=0$) and relaxed ($\rho=3$) precision and recall scores are used to evaluate the prediction results. Here the relaxed precision means the predicted pixels are within ρ pixels of a true pixel while the relaxed recall is the true pixels are within ρ pixels of a predicted pixel. Moreover, the time cost is used to measure the efficiency of our HF-FCN. For dataset *b*) and *c*), we use correctness, completeness and F1 score as evaluation metrics.

$$\text{completeness} = \frac{TP}{TP + FN}, \quad (8)$$

$$\text{correctness} = \frac{TP}{TP + FP}, \quad (9)$$

$$F1\text{score} = 2 \cdot \frac{\text{completeness} \cdot \text{correctness}}{\text{completeness} + \text{correctness}} \quad (10)$$

TABLE II
PARAMETERS FOR NETWORK TRAINING

	Massachusetts	Vaihingen	Potsdam
mini-batch size	18	15	15
initial learning rate	10^{-5}	10^{-6}	10^{-5}
test_interval	1000	1000	1000
training iteration	10000	10000	10000
momentum	0.9	0.9	0.9
clip_gradients	16000	10000	10000
weight_decay	0.02	0.005	0.005

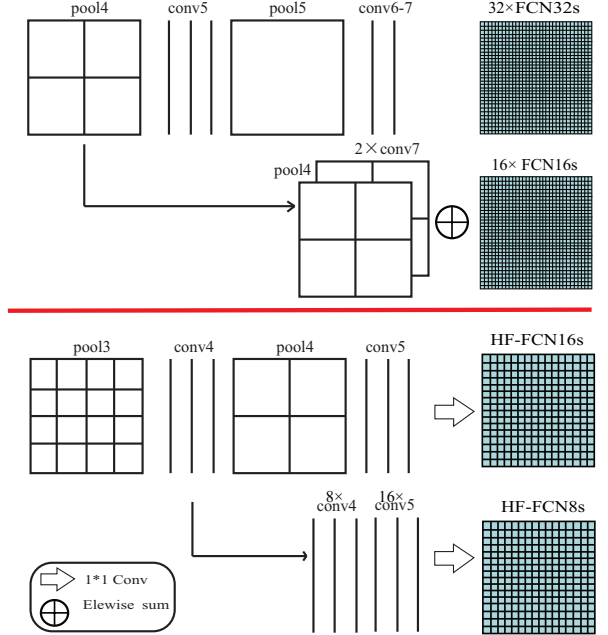


Fig. 5. FCN and HF-FCN variants. The feature maps generated from final group are fused into a coarse result, which is HF-FCN16s. The variant called HF-FCN8s concatenates the feature maps from the last 2 groups with the same fusion operation, and so on.

where TP indicates the true positives, FP implies the false positive, TN means the true negatives and FN refers to the false negatives.

V. RESULTS AND DISCUSSION

In this section, the proposed method using dataset *a*), *b*), *c*) is not only compared to the recent non-deep-learning algorithms, such as Minh-CNN [9], Satio-multi [10] and Context [15], but also compared with some recent deep-learning based approaches, including FCN [18], SegNet [19], Deeplab [21] and U-Net [29].(xuejin:What else?) Moreover, for HF-FCN itself, we expect to investigate which kind of information extracted from feature extractors and how the effects of extracted information on the final prediction. Thus, some upsampled feature maps $\{U_k\}$ are presented. And several variants of HF-FCN which combine different up-sampling feature maps from Part 2 are proposed. For dataset *b*) and *c*), multichannel information is provided. Hence, to explore the impact of other information on the results, a simple experiment is presented which concatenate different kinds of information as input of HF-FCN. In addition, different feature extractor networks are tried as our Part 1 network, including VGG16 Net and ResNet. The results and discussion of above mentioned experiments are shown below. (xuejin:What about to change the backbone network?)

A. Massachusetts dataset

On the Massachusetts dataset, both the non-deep-learning algorithms and deep-learning based approaches are compared with our method. Table III(xuejin:4) presents the quantitative analysis with a standard and relaxed precision and recall as evaluation criterions. The best results of our methods and

TABLE III
CORRECTNESS AT BREAKEVEN OF HF-FCN v.s. [9] [10] [11] [18] [19]
[29] [21] ON MASSACHUSETTS TEST SET. COST TIME IS COMPUTED IN
THE SAME COMPUTER WITH A SINGLE NVIDIA TITAN 12GB GPU

	Recall ($\rho = 3$)	Recall ($\rho = 0$)	Time (s)
Mnih-CNN [9]	0.9271	0.7661	8.70
Mnih-CNN+CRF [9]	0.9282	0.7638	26.60
Satio-multi-MA [10]	0.9503	0.7873	67.72
Satio-multi-MA&CIS [10]	0.9509	0.7872	67.84
Alshehhi-GAP+seg [11]	0.955	—	—
FCN_4s [18]	0.839	0.6147	4.20
SegNet [19]	0.7710	0.5675	2.39
U-Net [29]	0.9638	0.8357	3.165
DeepLab_V2 [21]	0.9620	0.7575	1.89
HF-FCN(VGG16 Net)	0.9643	0.8424	1.07
HF-FCN(VGG+data aug)	0.9650	0.8357	1.38
HF-FCN(ResNet)	0.9588	0.8175	2.42
HF-FCN16s	0.9330	0.7233	0.85
HF-FCN8s	0.9643	0.8171	0.93
HF-FCN4s	0.9632	0.8394	0.99

others' methods are marked in bold. From the view of result, our method shows obvious superiority in terms of speed and precision. When comparing with Satio-multi-MA&CIS [10], the standard and relaxed recall of our method are 5.5% and 1.3% higher than it. Meanwhile, the time cost is reduced from 67.84s to 1.07s and the speed is promoted about 63 times. These significant improvements demonstrate that HF-FCN achieves better performance in effectiveness and efficiency.

Extensive comparisons are made between HF-FCN and other semantic segmentation methods. The quantitative and visual results are shown in Table III and Fig. 9, respectively. Compared with U-Net [29], the speed is promoted about 3 times and recall is a little higher. From the visual results, our method preserve the details and integrity of the building better than others.

In addition, to explore which kinds of information extracted by hierarchical fusion operation in Part 2. Some upsampled feature maps $\{U_1, U_2, U_3, U_7, U_{10}, U_{13}\}$ are shown in Fig. 6. The U_{1_1} (U_1) in Fig. 6(b) means the upsampled feature map from F_{1_1} (F_1) which are feature maps generated from conv1_1 in VGG16 Net. Due to small receptive field of conv1_1 and conv1_2, they extract low-level features like edges. And the U_{1_2} (U_2) looks like an over-segmentation which groups pixels with similar color or texture into a subregion. With the deepening of the network, in the U_{2_1} (U_3), as Fig. 6(d) shows, shape information is augmented. And from the U_{3_3} (U_7), we can see that regions with significantly varying appearance are merged into an integrated building by considering high-level features. In U_{4_3} (U_{10}) and U_{5_3} (U_{13}), more semantic information of rooftop is got, which can distinguish the rooftop and the roads with similar color and deal with the problem caused by shadow. The final prediction results are shown in Fig. 6(h).

Secondly, to explore the effects of the feature maps generated from each feature extract stage $\{F_k\}$ on the final result, variants of HF-FCN which are counterpart of FCN are designed. Fig. 5 shows the contrast diagram of variants of FCN and HF-FCN. Unlike FCN, a fusion operation rather than summation are leveraged to build our HF-FCN 16s, 8s and 4s. The precision-recall(PR) curves, prediction results and

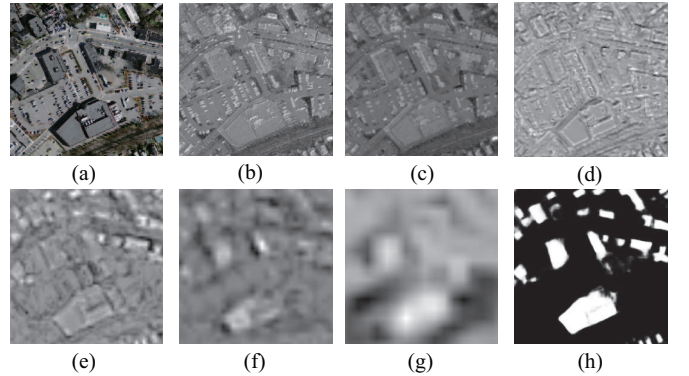


Fig. 6. (a) Input aerial image. (b-g) Feature maps of U_{1_1} , U_{1_2} , U_{2_1} , U_{3_3} , U_{4_3} , U_{5_3} , respectively. (h) Predicted label map. All the images are normalized to the range of 0 – 255.

quantitative results of HF-FCN variants are shown in Fig. 7, Fig. 8 and Table III respectively. (xuejin:Figure 8, Figure 9 and Table V). From the diagrams, we can get the following conclusions easily:

- The prediction result obtained from the last layer gets a coarse result, which loses much of location information that are mainly encoded in the shallow feature maps.
- The largest gap presented between HF-FCN16s and HF-FCN8s about 9% in recall rates, it may suggest that the most information supplement to the HF-FCN is got in middle layers.
- The PR curves of HF-FCN4s and HF-FCN almost coincide. It illustrates the low-level information has little effect on the prediction results.
- with the addition of the shallow feature map, the network is more distinct for the segmentation of tiny buildings, which solves the problem of easy adhesion to adjacent buildings.

Since, all the feature maps contained useful hierarchical information that is critical to the final prediction.

In the end, we want to prove that our fusion operations learn the connections between feature maps. The connection weights of F_{1_1} , F_{4_1} and Part 3 are shown in Fig. 10. The weights are not the same, which means that fusion operations have effect on feature combination. From the Fig. 10 (a) to Fig. 10 (c), the range of weights increases gradually. And from the Fig. 10 (c), we can arrive at the conclusion that the different layers have virous effects on the final result. For example, the U_{1_1} has little effect on the prediction while the U_{3_2} and U_{4_3} play more important roles on the final prediction. It also in accordance with our experimental results that middle layers provide more information. (xuejin:Weight for what? to fuse feature map? The distribution does not make too much sense.)

B. Vaihingen dataset

On Vaihingen dataset, three experiments are undertaken to explore the effects of different inputs, diverse variants and various methods. Three kinds of combinations of image channels are utilized as inputs. The inputs of the 3 channels

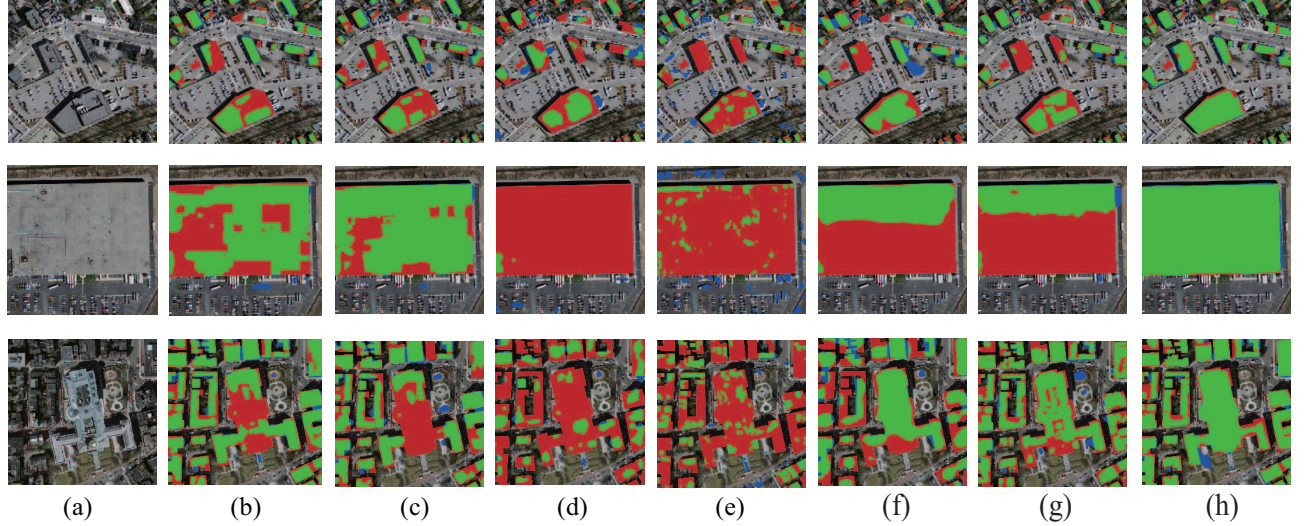


Fig. 9. (a) input images. (b) Results of Mnih-CNN+CRF. (c) Results of SatiomultiMA&CIS. (d) Results of FCN4s . (e) Results of SegNet. (f) Results of DeepLab_V2. (g) Results of U-Net. (h) Our results. TP are shown in green, FP are shown in blue and FN are in red.

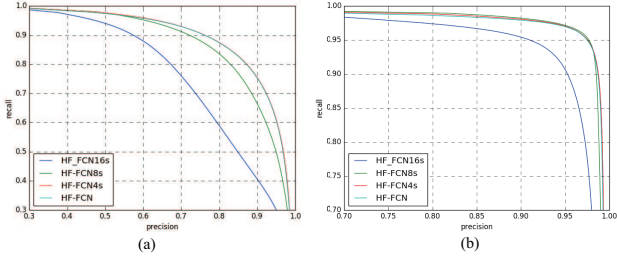


Fig. 7. The relaxed PR curves from HF-FCN variants with two slack parameters. The slack parameter ρ on the left is 0. And $\rho = 3$ on the right.

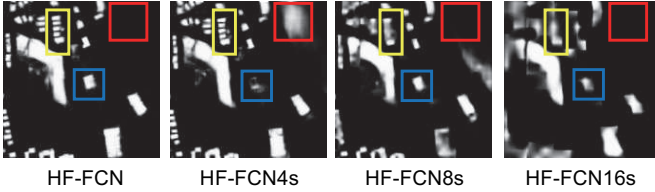


Fig. 8. Prediction results of HF-FCN, HF-FCN4s, HF-FCN8s and HF-FCN16s. The yellow box shows the continuous refinement of the tiny buildings. The red and blue boxes show the mutual promotion and contradiction between different layers.

are IR, R, G and adding the nDSM(normalized Digital Surface Model) as the forth channel. Based on it, DSM is added and made up 5-channel input. Three standards are used to make a more comprehensive evaluation. The evaluation results are shown in Table IV, which illustrate that 3-channel input performed better than the others. The Rec and Pre in Table IV

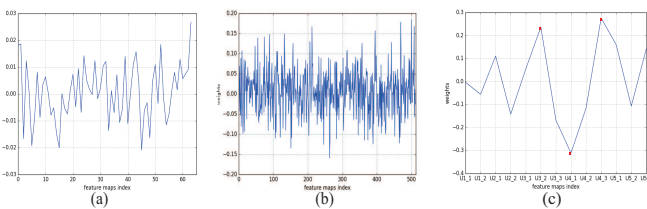


Fig. 10. (a) is weights learned by F1_1, (b) is weights learned by F4_1, (c) is weights learned by Part 3.

means the recall and precision of prediction results. And F1 indicates the F1 score of results. The number in bold shows the best results of our methods and other methods. Visual results of our methods with different kinds of input are shown in Fig. 13.

(xuejin:Do you compare with others?)

TABLE IV
PERFORMANCE COMPARISON OF THE RESULTS OF DIFFERENT INPUTS AND METHODS ON VAIHIGEN DATA SET. (XUEJIN:WHAT ARE THE NUMBERS IN THE IMG COLUMN?)

		Pre	Rec	F1
Val	3_in	0.939	0.894	0.915
	4_in	0.96	0.865	0.909
	5_in	0.939	0.880	0.907
Test	3_in	0.919	0.930	0.925
	4_in	0.907	0.872	0.888
	5_in	0.858	0.900	0.878
FCN_4s [18]	0.871	0.884	0.878	
SegNet [19]	0.917	0.861	0.887	
U-Net [29]	0.848	0.737	0.789	
DeepLab_V2 [21]	0.926	0.881	0.903	
HF-FCN16s	0.886	0.854	0.870	
HF-FCN8s	0.911	0.864	0.887	
HF-FCN4s	0.910	0.861	0.885	

Many experiments are done to compare with other methods, including methods using the same dataset and the other deep learning based methods. The detail comparison results using the same dataset are shown in Fig. 14. From a visual perspective, our method gets a much more refined roof region, both on continuity of labels and integrity of structural. The quantitative results of deep learning methods are shown in Table IV. Compared to DeepLab_V2 [21], the F1 score of our method improves 2.2%.

The results of diverse variants are shown in Fig. 11. The HF-FCN_1 in Fig. 11 indicates that the last conv layer in Part 3 does not use the previous trained model to initialize. And HF-FCN means that the whole layers use the pre-trained model to initialize. From the curves, the performance of HF-FCN exceeds the variants and gets a excellent result. Additionally,

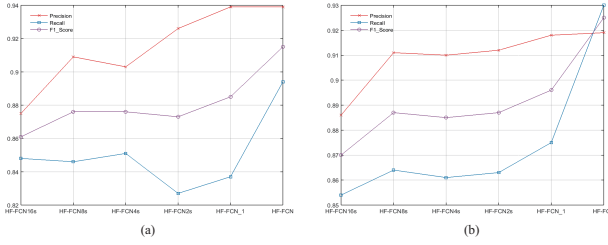


Fig. 11. Results of HF-FCN variants on Vaihingen dataset. (a) (b) shows the precision, recall and F1 score of validation set and test set of Vaihingen dataset respectively.(xuejin:Bigger font)

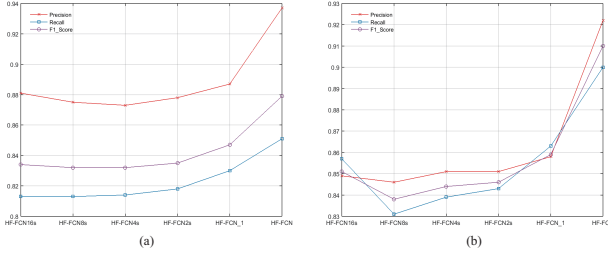


Fig. 12. Results of HF-FCN variants on Potsdam dataset. (a) (b) shows the precision, recall and F1 score of validation set and test set of Potsdam dataset respectively.

using the pre-trained weights of Part 3 has a significance in the final results.

C. Potsdam dataset

The same experiments are implemented on Potsdam dataset, including effects of different channels of input, comparing with other methods and results of diverse variants of HF-FCN. Firstly, we utilize nDSM and IR information as extra inputs based on the RGB input. The specific quantitative evaluation and intuitive visual prediction results are shown in Table V and Fig. 15. In the validation process, the 4-channel input including

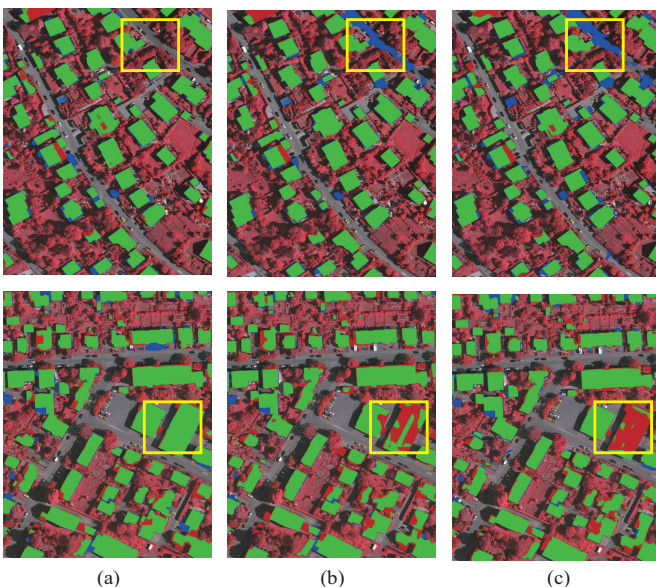


Fig. 13. Prediction results on Vaihingen dataset. (a) (b) (c) shows results of the 3-channel input, 4-channel input and 5-channel input of Vaihingen dataset respectively. Here, TP are shown in green, FP are shown in blue and FN are in red.

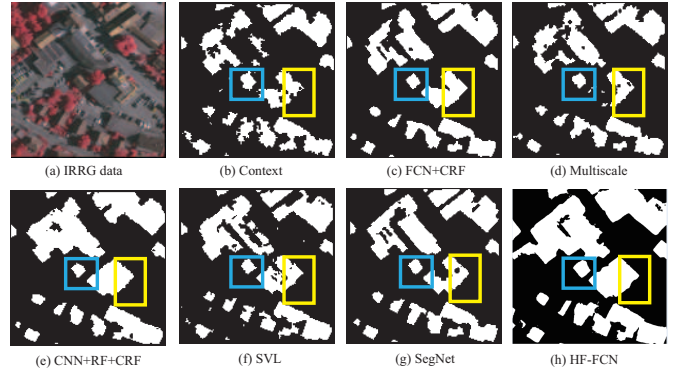


Fig. 14. Results of different methods. (a) is input image, (b)-(d)(g) are results of [15], (e) is result of [31], (f) is result of [32], (g) is our result. The blue and yellow frames show some details between these methods.

RGB, nDSM gets better overall performance. Meanwhile, the 5-channel input including RGB, nDSM and IR seems perform better in the course of testing. From the visual results, the 5-channel input network gets lower error detection rate which is shown on the image with small blue areas. And from the 3-channel input to 5-channel input, the F1 score increases from 0.879 to 0.891 on the validation set and increases 0.031 on the test set. It indicate that the other information of geographical feature have a certain effect on the final result.

We compare HF-FCN with other methods using the Potsdam dataset and several deep learning methods. Some qualitative results of methods using Potsdam dataset are shown in Fig. 16. From the figure, we can easily see that HF-FCN got more remarkable segmentation results. And edges and structure of buildings are preserved better. The results of deep learning methods are shown in Table V. From the Table, the HF-FCN achieves the best result. And the F1 score far higher than the others.

As done on Vaihingen dataset, contrast experiments of HF-FCN variants are implemented. The performance curve of HF-FCN variants are shown in Fig. 12. The HF-FCN_1 in Fig. 12 indicates that the last conv layer in Part 3 does not use the previous trained model to initialize. And HF-FCN means that the whole layers use the pre-trained model to initialize. Initialization of parameters has a greater promotion on the final results.

TABLE V
PERFORMANCE COMPARISON OF THE RESULTS OF DIFFERENT INPUTS
AND METHODS ON POTSDAM DATA SET

		Pre	Rec	F1
Val	3_in	0.937	0.851	0.879
	4_in	0.937	0.872	0.894
	5_in	0.944	0.864	0.891
Test	3_in	0.922	0.900	0.910
	4_in	0.937	0.935	0.936
	5_in	0.940	0.943	0.941
	FCN_4s [18]	0.827	0.774	0.796
	SegNet [19]	0.648	0.773	0.687
	U-Net [29]	0.924	0.705	0.799
	DeepLab_V2 [21]	0.901	0.876	0.887
	HF-FCN16s	0.849	0.857	0.851
	HF-FCN8s	0.846	0.831	0.838
	HF-FCN4s	0.851	0.839	0.844

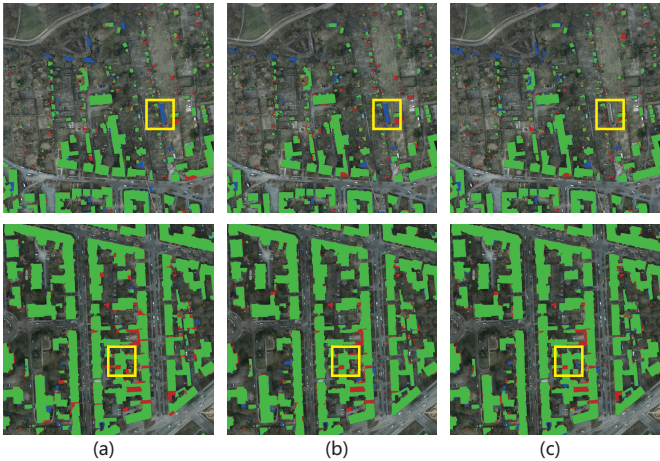


Fig. 15. Prediction results on potsdam dataset. (a) (b) (c) shows results of the 3-channel input, 4-channel input and 5-channel input of Vaihingen dataset respectively. Here, TP are shown in green, FP are shown in blue and FN are in red.

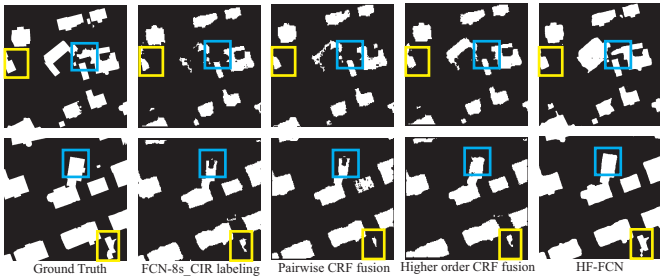


Fig. 16. Results of different methods. The second column is the results of using only the FCN with CIR(color-infrared image). Pairwise CRF fusion shows the result of fusing FCN-8s_CIR with LiDAR data in a pairwise CRF. The results of using higher-order CRF [14] as post processing are shown in third column. The last column shows our results.

VI. APPLICATION

The segmentation results are further used to 3D building reconstruction. We make use of the depth map and generate the point cloud of remote sensing images. After that, the 3D building reconstruction methods could applied to the generated point cloud. In this paper, the approach proposed by zhou [33] are used to generate the 3D models of buildings in the scene. Fig. 17 and Fig. 18 show the 3D models of Vaihingen and Potsdam dataset respectively. The details of a single building are also presented. From the figures, we can see that 3D models preserve the characteristics of buildings well whether the structure of the roof or the simplification of details.

VII. CONCLUSION

In this paper, an efficient building detection approach is proposed and have a further application in building reconstruction. Using proposed feature fusion operations, a novel CNN architecture is presented for building extraction, named HF-FCN. Unlike previous non-deep-learning algorithms, we provide an end-to-end network for building extraction. And it is robust to the different scales of buildings and efficient for a large-scale remote sensing images. On the other hand, distinct from the previous deep learning based methods, we utilize the multi-scale inherent information within the CNN

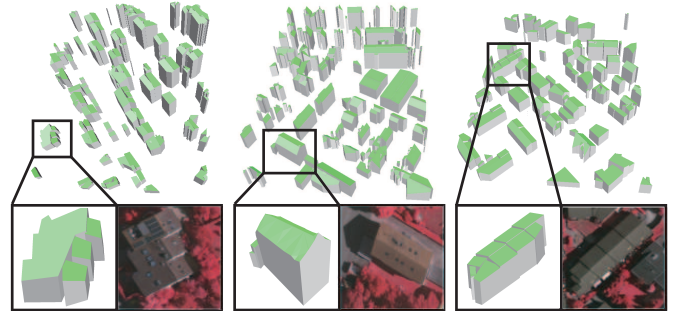


Fig. 17. The 3D modelling of Vaihingen dataset. The single building model and its corresponding optical patch were shown together.

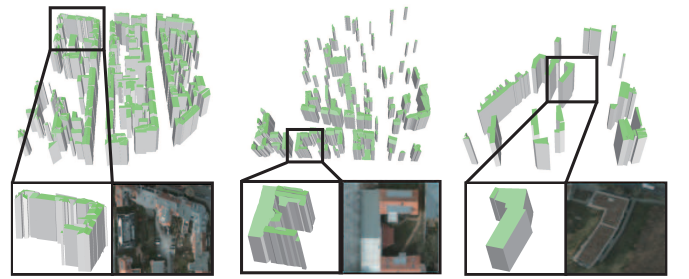


Fig. 18. The 3D modelling of Potsdam dataset. The single building model and its corresponding optical patch were shown together.

and refine the details by a fusion manner stage by stage. In addition, an application of 3D building reconstruction depend on the segmentation results is implemented. Finally, our study suggests that even with the powerful semantic expressive ability of CNNs and their good robustness to scale, it is still critical to address multi-scale building extraction problem by utilizing hierarchical feature maps encoded in CNNs.

REFERENCES

- [1] A. Huertas and R. Nevatia, "Detecting buildings in aerial images," *Computer Vision, Graphics, and Image Processing*, vol. 41, no. 2, pp. 131–152, 1988.
- [2] S. Noronha and R. Nevatia, "Detection and modeling of buildings from multiple aerial images," *IEEE Transactions on pattern analysis and machine intelligence*, vol. 23, no. 5, pp. 501–518, 2001.
- [3] M. S. Nosrati and P. Saeedi, "A novel approach for polygonal rooftop detection in satellite/aerial imageries," in *Image Processing (ICIP), 2009 16th IEEE International Conference on*. IEEE, 2009, pp. 1709–1712.
- [4] M. Izadi and P. Saeedi, "Three-dimensional polygonal building model estimation from single satellite images," *IEEE Transactions on Geoscience and Remote Sensing*, vol. 50, no. 6, pp. 2254–2272, 2012.
- [5] J. Wang, X. Yang, X. Qin, X. Ye, and Q. Qin, "An efficient approach for automatic rectangular building extraction from very high resolution optical satellite imagery," *IEEE Geoscience and Remote Sensing Letters*, vol. 12, no. 3, pp. 487–491, 2015.
- [6] M. Cote and P. Saeedi, "Automatic rooftop extraction in nadir aerial imagery of suburban regions using corners and variational level set evolution," *IEEE transactions on geoscience and remote sensing*, vol. 51, no. 1, pp. 313–328, 2013.
- [7] J. Peng, D. Zhang, and Y. Liu, "An improved snake model for building detection from urban aerial images," *Pattern Recognition Letters*, vol. 26, no. 5, pp. 587–595, 2005.
- [8] B. Sirmacek and C. Unsalan, "Urban-area and building detection using sift keypoints and graph theory," *IEEE Transactions on Geoscience and Remote Sensing*, vol. 47, no. 4, pp. 1156–1167, 2009.
- [9] V. Mnih, "Machine learning for aerial image labeling," Ph.D. dissertation, University of Toronto (Canada), 2013.
- [10] S. Saito, T. Yamashita, and Y. Aoki, "Multiple object extraction from aerial imagery with convolutional neural networks," *Electronic Imaging*, vol. 2016, no. 10, pp. 1–9, 2016.

- [11] R. Alshehhi, P. R. Marpu, W. L. Woon, and M. Dalla Mura, "Simultaneous extraction of roads and buildings in remote sensing imagery with convolutional neural networks," *ISPRS Journal of Photogrammetry and Remote Sensing*, vol. 130, pp. 139–149, 2017.
- [12] W. Zhao, S. Du, Q. Wang, and W. J. Emery, "Contextually guided very-high-resolution imagery classification with semantic segments," *ISPRS Journal of Photogrammetry and Remote Sensing*, vol. 132, pp. 48–60, 2017.
- [13] S. Paisitkriangkrai, J. Sherrah, P. Janney, V.-D. Hengel *et al.*, "Effective semantic pixel labelling with convolutional networks and conditional random fields," in *Proceedings of the IEEE Conference on Computer Vision and Pattern Recognition Workshops*, 2015, pp. 36–43.
- [14] Y. Liu, S. Piramanayagam, S. T. Monteiro, and E. Saber, "Dense semantic labeling of very-high-resolution aerial imagery and lidar with fully-convolutional neural networks and higher-order crfs," in *Proceedings of the IEEE Conference on Computer Vision and Pattern Recognition Workshops*, 2017, pp. 76–85.
- [15] N. Audebert, A. Boulch, H. Randrianarivo, B. Le Saux, M. Ferecatu, S. Lefevre, and R. Marlet, "Deep learning for urban remote sensing," in *Urban Remote Sensing Event (JURSE), 2017 Joint*. IEEE, 2017, pp. 1–4.
- [16] M. Kampffmeyer, A.-B. Salberg, and R. Jenssen, "Urban land cover classification with missing data using deep convolutional neural networks," *arXiv preprint arXiv:1709.07383*, 2017.
- [17] Y. He, S. Mudur, and C. Poullis, "Multi-label pixelwise classification for reconstruction of large-scale urban areas," *arXiv preprint arXiv:1709.07368*, 2017.
- [18] J. Long, E. Shelhamer, and T. Darrell, "Fully convolutional networks for semantic segmentation," in *The IEEE Conference on Computer Vision and Pattern Recognition (CVPR)*, June 2015.
- [19] V. Badrinarayanan, A. Kendall, and R. Cipolla, "Segnet: A deep convolutional encoder-decoder architecture for scene segmentation," *IEEE transactions on pattern analysis and machine intelligence*, 2017.
- [20] J. Hoffman, S. Gupta, and T. Darrell, "Learning with side information through modality hallucination," in *Proceedings of the IEEE Conference on Computer Vision and Pattern Recognition*, 2016, pp. 826–834.
- [21] L.-C. Chen, G. Papandreou, I. Kokkinos, K. Murphy, and A. L. Yuille, "Deeplab: Semantic image segmentation with deep convolutional nets, atrous convolution, and fully connected crfs," *arXiv preprint arXiv:1606.00915*, 2016.
- [22] R. Vemulapalli, O. Tuzel, M.-Y. Liu, and R. Chellappa, "Gaussian conditional random field network for semantic segmentation," in *Proceedings of the IEEE Conference on Computer Vision and Pattern Recognition*, 2016, pp. 3224–3233.
- [23] K. He, X. Zhang, S. Ren, and J. Sun, "Deep residual learning for image recognition," in *Proceedings of the IEEE conference on computer vision and pattern recognition*, 2016, pp. 770–778.
- [24] C. Szegedy, W. Liu, Y. Jia, P. Sermanet, S. Reed, D. Anguelov, D. Erhan, V. Vanhoucke, and A. Rabinovich, "Going deeper with convolutions," in *Proceedings of the IEEE conference on computer vision and pattern recognition*, 2015, pp. 1–9.
- [25] C. Szegedy, V. Vanhoucke, S. Ioffe, J. Shlens, and Z. Wojna, "Rethinking the inception architecture for computer vision," in *Proceedings of the IEEE Conference on Computer Vision and Pattern Recognition*, 2016, pp. 2818–2826.
- [26] C. Szegedy, S. Ioffe, V. Vanhoucke, and A. A. Alemi, "Inception-v4, inception-resnet and the impact of residual connections on learning," in *AAAI*, 2017, pp. 4278–4284.
- [27] S. Xie, R. Girshick, P. Dollár, Z. Tu, and K. He, "Aggregated residual transformations for deep neural networks," in *2017 IEEE Conference on Computer Vision and Pattern Recognition (CVPR)*. IEEE, 2017, pp. 5987–5995.
- [28] T. Zuo, J. Feng, and X. Chen, "Hf-fcn: Hierarchically fused fully convolutional network for robust building extraction," in *Asian Conference on Computer Vision*. Springer, 2016, pp. 291–302.
- [29] O. Ronneberger, P. Fischer, and T. Brox, "U-net: Convolutional networks for biomedical image segmentation," in *International Conference on Medical Image Computing and Computer-Assisted Intervention*. Springer, 2015, pp. 234–241.
- [30] T.-Y. Lin, P. Dollár, R. Girshick, K. He, B. Hariharan, and S. Belongie, "Feature pyramid networks for object detection," in *CVPR*, vol. 1, no. 2, 2017, p. 4.
- [31] D. Marmanis, J. D. Wegner, S. Galliani, K. Schindler, M. Datcu, and U. Stilla, "Semantic segmentation of aerial images with an ensemble of cnns," *ISPRS Annals of the Photogrammetry, Remote Sensing and Spatial Information Sciences*, 2016, vol. 3, pp. 473–480, 2016.
- [32] M. Gerke, "Use of the stair vision library within the isprs 2d semantic labeling benchmark (vaihingen)," 01 2015.
- [33] Q.-Y. Zhou and U. Neumann, "2.5 d building modeling with topology control," in *Computer Vision and Pattern Recognition (CVPR), 2011 IEEE Conference on*. IEEE, 2011, pp. 2489–2496.